Physics of the Earth and Planetary Interiors 268 (2017) 65–77

Contents lists available at ScienceDirect

Physics of the Earth and Planetary Interiors

journal homepage: www.elsevier.com/locate/pepi

Impact of compressibility on heat transport characteristics of large terrestrial planets

Hana Čížková [a,*], Arie van den Berg [b,c], Michel Jacobs [d]

[a] Charles University, Faculty of Mathematics and Physics, Department of Geophysics, Czech Republic
[b] Utrecht University, Institute of Earth Sciences, Department of Theoretical Geophysics, Netherlands
[c] Vrije Universiteit Amsterdam, Faculty of Earth and Life Sciences, Netherlands
[d] TU Clausthal, Institut für Metallurgie, Germany

ARTICLE INFO

Article history:
Received 16 August 2016
Received in revised form 12 April 2017
Accepted 26 April 2017
Available online 10 May 2017

Keywords:
Compressible mantle convection
Terrestrial exoplanets
Heat transport

ABSTRACT

We present heat transport characteristics for mantle convection in large terrestrial exoplanets ($M \leqslant 8M_{\oplus}$). Our thermal convection model is based on a truncated anelastic liquid approximation (TALA) for compressible fluids and takes into account a selfconsistent thermodynamic description of material properties derived from mineral physics based on a multi-Einstein vibrational approach. We compare heat transport characteristics in compressible models with those obtained with incompressible models based on the classical- and extended Boussinesq approximation (BA and EBA respectively). Our scaling analysis shows that heat flux scales with effective dissipation number as $Nu \sim Di_{eff}^{-0.71}$ and with Rayleigh number as $Nu \sim Ra_{eff}^{0.27}$. The surface heat flux of the BA models strongly overestimates the values from the corresponding compressible models, whereas the EBA models systematically underestimate the heat flux by ~10%–15% with respect to a corresponding compressible case. Compressible models are also systematically warmer than the EBA models. Compressibility effects are therefore important for mantle dynamic processes, especially for large rocky exoplanets and consequently also for formation of planetary atmospheres, through outgassing, and the existence of a magnetic field, through thermal coupling of mantle and core dynamic systems.

1. Introduction

Recent progress in detection techniques resulted in discoveries of numerous terrestrial (rocky) exoplanets (eg. Mayor et al., 2009; Fressin et al., 2012; Batalha et al., 2013). This has inspired an increasing number of studies focused on their internal dynamics (e.g. Valencia et al., 2006; van den Berg et al., 2010; Tachinami et al., 2011; Tackley et al., 2013). Mantle dynamics of terrestrial (exo) planets has traditionally been studied in terms of incompressible Boussinesq models (e.g. Behounková et al., 2010; de Vries et al., 2010; van den Berg et al., 2010; van Summeren et al., 2011; van and Tackley, 2011; Stamenkovic et al., 2011).

These models may be reasonably applicable to the Earth and planets of a comparable or smaller size, where the effects of compressibility are relatively small. They have however also been applied to larger planetary bodies where pressure and resulting selfcompression are much higher than in the Earth's mantle.

These incompressible models have provided various insights into convection characteristics e.g. in models including selfconsistently generated plate tectonics, and rheological weakening in the lower mantle (van and Tackley, 2011; Foley et al., 2012; Stein et al., 2011), the impact of phase transitions and variable thermal conductivity at higher P,T conditions in exoplanets (van den Berg et al., 2010), and the mantle dynamical consequence of strong external heating in terrestrial planets in close orbit around their parent star (van Summeren et al., 2011).

Since the mantles of the larger rocky exoplanets are subject to considerably stronger compression than experienced in the Earth the application of incompressible models may be questionable.

As shown by Jarvis and McKenzie (1980) and Steinbach (1991), the critical Rayleigh number (Ra_c) increases with increasing dissipation number (Di) and convection is getting more stable and thus the vigour and perhaps even the presence of convection are under question in the deep mantle of large planetary bodies. In line with this a number of studies, that are focused on the effects of compressibility on mantle convection in large exoplanetary bodies, have recently appeared. Scaling relations that characterise heat transport efficiency expressed by the Nusselt number (Nu) as a

* Corresponding author at: Department of Geophysics, V Holešovičkách 2, 180 00 Prague 8, Czech Republic.
E-mail address: Hana.Cizkova@mff.cuni.cz (H. Čížková).

http://dx.doi.org/10.1016/j.pepi.2017.04.007
0031-9201/

function of Ra and Di were derived for different parameterised equations of state both for constant and depth dependent thermal expansivity (Liu and Zhong, 2013; Miyagoshi et al., 2015). Heat transport efficiency was reported to increase as $Ra^{1/3}$ similarly to incompressible models while it decreases strongly with increasing Di – Nu is 25× lower in case of Di = 2 than in the corresponding endmember case Di = 0 of the incompressible classical Boussinesq model (Liu and Zhong, 2013). For higher values of standard dissipation number, Di $>\sim$ 2, characteristic for planets 5 times more massive than Earth, convection does not occur for constant expansivity (Tachinami et al., 2014) and a pressure dependent expansivity decreasing with increasing pressure/depth, in line with mineral physics, is necessary to allow for convective heat transport.

Here we investigate four model planets with increasing mass (Earth-like and two, four and eight times the Earth's mass) and corresponding depth of the mantle under compression which involves that they also have different dissipation numbers (increasing from 0.8 to 2.5). Common approaches of modelling compressible media use parameterized material properties and in order to reduce the number of parameters the thermodynamic Grueneisen parameter is constrained to a representative (for example unit) value, thereby eliminating the incompressibility as an independent parameter (e.g. Jarvis and McKenzie, 1980; Steinbach, 1991; Leng and Zhong, 2008; King et al., 2010; Liu and Zhong, 2013). This way it is not possible to investigate compressibility effects separately from the dissipation effects by varying compressibility independently from the dissipation number (see Appendix for more details). Here we take a different approach and for a given material composition (a mechanical mixture of specific minerals) we apply corresponding selfconsistent thermophysical material properties based on a multi-einstein vibrational approach (Ita and King, 1994; Jacobs et al., 2016). This way density, thermal expansivity and heat capacity are all pressure and temperature dependent.

We investigate model behavior under different pressure/compression conditions representative of large terrestrial planets for a range of planet mass values. To this end we compute planetary internal structure such as mantle depth d and radial profiles of density, gravity and pressure of these model planets in a consistent way, applying a thermal equation of state for density as further explained in Section 3. We use the planetary mass M as a control parameter in our convection modelling experiments. Planet mass is closely linked to the standard dissipation number $Di = \alpha_0 g_0 d/c_{p0}$ through the layer depth $d(M)$.

A crucial parameter that affects convective vigour and heat transport efficiency is the viscosity. Compressible convection experiments with purely temperature dependent viscosity in a large exoplanet with a mass 10 times the Earth mass (Miyagoshi et al., 2014; Miyagoshi et al., 2015) show a decrease in heat transport efficiency with increasing viscosity contrast, but they neglect viscosity variations induced by pressure. The effect of pressure on viscosity in the very high pressure regime is not well constrained and inferrences of viscosity in the lower mantle of large exoplanets are ambiguous (Ammann et al., 2010; Karato, 2011; Stamenkovic et al., 2011; Tackley et al., 2013; Noack and Breuer, 2014).

Therefore we first investigate the effect of the thermophysical parameters density, thermal expansivity and specific heat at constant pressure in compressible models while keeping the viscosity constant. This constant viscosity is here applied to control the Rayleigh number thereby focussing on the effects of compressibility. In a second set of experiments we include variable P,T dependent viscosity to test the robustness of our findings for constant viscosity models under conditions with highly variable viscosity.

In our experiments we focus on evaluating the differences between compressible models with P,T dependent material properties and incompressible Boussinesq models with properties that are purely pressure dependent, for mantle models that are representative of large terrestrial exoplanets.

2. Method

Equations describing infinite Prandtl number thermal convection in a compressible mantle under the assumptions of the Anelastic Liquid Approximation (ALA) differ from incompressible models by including density in the continuity equation and by adding the divergence of velocity in the constitutive relation. The continuity equation then reads

$$\nabla \cdot (\rho_r \mathbf{v}) = 0, \tag{1}$$

where ρ_r is a depth dependent reference density and $\mathbf{v}$ is the flow velocity. The (Stokes) momentum equation is

$$\nabla \cdot \boldsymbol{\sigma} - \nabla P + \rho \mathbf{g} = 0, \tag{2}$$

where $\boldsymbol{\sigma}$ is deviatoric stress, P is the thermodynamic (total) pressure and $\mathbf{g}$ the gravity acceleration vector. Density and pressure are rewritten in terms of perturbations with respect to one-dimensional pressure/depth dependent reference profiles in,

$$\rho(P,T) = \rho_r(P) + \Delta\rho(P,T) \tag{3}$$

$$P(\mathbf{x}) = P_r(z) + p(\mathbf{x}), \nabla P_r = \rho_r \mathbf{g}, \tag{4}$$

where p is the dynamic pressure, $\mathbf{x}$ the spatial coordinate vector and z is the depth below the zero pressure top surface. Rewriting the Stokes Eq. (2) in terms of the driving perturbations, $p, \Delta\rho$ we get,

$$\nabla \cdot \boldsymbol{\sigma} - \nabla p + \Delta\rho \mathbf{g} = 0, \tag{5}$$

The density $\rho(P,T)$ is a function of temperature T and thermodynamic pressure P. As in (Jacobs and van den Berg, 2011) this function is represented in P,T tabular form for the P,T region of interest. Note that the formulation in (5) does not make use of linearization of the effect of thermal expansivity on density in terms of the thermal expansion coefficient.

A further approximation is introduced in our model by neglecting the effect of dynamic pressure p in the interpolations from the look-up table for $\rho(P,T)$, by setting $P(\mathbf{x}) = P_r(z(\mathbf{x}))$ This comes down to applying the truncated anelastic liquid approximation (TALA) (Leng and Zhong, 2008).

The energy transport equation is,

$$\rho c_p \frac{DT}{Dt} - \alpha \rho g T v_z = \nabla \cdot (k \nabla T) + \boldsymbol{\sigma} : \nabla \mathbf{v}, \tag{6}$$

with c_p specific heat at constant pressure, T temperature, t time, k thermal conductivity, α thermal expansivity and v_z is the downward velocity component, aligned with gravity. Internal heating due to radioactive decay is not taken into account. We assume a linear viscous rheology

$$\sigma_{ij} = \eta \left(\frac{\partial v_i}{\partial x_j} + \frac{\partial v_j}{\partial x_i} - \frac{2}{3} \nabla \cdot \mathbf{v} \delta_{ij} \right). \tag{7}$$

The viscosity is constant $\eta = \eta_0$ in most models runs. In order to estimate the effects of a p,T-dependent rheology we also apply the following variable viscosity model adopted from (Tackley et al., 2013):

$$\eta(p,T) = \eta_r exp\left(\frac{H(p)}{RT} - \frac{H(0)}{RT_r} \right) \tag{8}$$

$$H(p) = E_0 + pV_0 exp\left(-\frac{p}{p_{decay}} \right) \tag{9}$$

where we apply activation parameters relevant for their lower bound post-perovskite rheology (see Table 1).

Table 1
Symbols and model parameters. The following scale values were used for both incompressible and compressibble models: expansivity, $\alpha_0 = 2.09 \times 10^{-5}$ K^{-1}, density, $\rho_0 = 4000$ kg m^{-3}, specific heat, $c_{p0} = 1250$ J K^{-1} kg^{-1}, thermal diffusivity, $\kappa_0 = 10^{-6}$ m^2 s^{-1}. Scale values of viscosity η_0 are given in Table 3 for individual models.

Symbol	Meaning	Value used	Dimension
α	thermal expansion coefficient		K^{-1}
$\alpha_{depth1} = \frac{\alpha_0 \Delta\alpha}{[(\Delta\alpha^{1/3}-1)(1-z)+1]^3}$	special case depth dependent α		K^{-1}
c_p	specific heat		J kg^{-1} K^{-1}
k	thermal conductivity	5	K m^2 s^{-1}
g	gravitatioal acceleration		m s^{-2}
$Di = \alpha_0 g_0 d / c_{p0}$	Standard dissipation number		–
$Ra = \rho_0 \alpha_0 g_0 \Delta T d^3 / \eta_0 \kappa_0$	thermal Rayleigh number		–
T	temperature		K
T_s	surface temperature	273	K
p	dynamic pressure		Pa
ΔT	top/bottom temperature contrast		K
t	time		s
$\mathbf{v}$	velocity		m s^{-1}
η	viscosity		Pa s
ρ	density		kg m^{-3}
ρ_r	reference density		kg m^{-3}
$P_r(z) = \int_0^z \rho_r g d\zeta$	reference pressure profile		Pa
z	depth below the top surface		m
σ_{ij}	deviatoric stress tensor		Pa
η_r	reference viscosity of pT dependent rheology	1.9×10^{21}	Pa s
V_0	activation volume	1.4	cm^3/mol
E_0	activation energy	162	kJ/mol
p_{decay}	pressure decay	1610	GPa
T_r	reference temperature	1600	K
R	gas constant	8.314	J K^{-1} mol^{-1}

We non-dimensionalize equations (5), (6) with the following scheme, denoting non-dimensional variables by primed symbols and using zero subscript for the scale values: spatial coordinates $\mathbf{x} = d\mathbf{x}'$, time $t = (d^2/\kappa_0)t'$, thermal diffusivity $\kappa = \kappa_0 = k_0/(\rho_0 c_{p0})$, density $\rho = \rho_0 \rho'$, specific heat at constant pressure $c_p = c_{p0} c_p'$, thermal expansivity $\alpha = \alpha_0 \alpha'$, gravity acceleration $\mathbf{g} = g_0 \mathbf{g}'$, Dynamic pressure and deviatoric stress are scaled by $p_0 = \eta_0 \kappa_0 / d^2$. Temperature is non-dimensionalized as $T = T_s + T' \Delta T$. Symbols and corresponding scale values are listed in Table 1.

Substitution in (5) and (6) and dropping the primes on non-dimensional variables, gives the non-dimensional momentum and energy tranport equations,

$$\nabla \cdot \boldsymbol{\sigma} - \nabla p + \frac{Ra}{\alpha_0 \Delta T} \Delta\rho \mathbf{g} = 0, \tag{10}$$

$$\rho c_p \frac{DT}{Dt} - \alpha \rho g Di v_z (T + T_s/\Delta T) = \nabla \cdot (k \nabla T) + \frac{Di}{Ra} \boldsymbol{\sigma} : \nabla \mathbf{v}, \tag{11}$$

The Rayleigh number, Ra, and dissipation number, Di, based on the scale values of model parameters follow from the non-dimensionalization scheme as,

$$Ra = \frac{\rho_0 \alpha_0 g_0 d^3 \Delta T}{\eta_0 \kappa_0} \tag{12}$$

$$Di = \frac{\alpha_0 g_0 d}{c_{p0}}. \tag{13}$$

In our models with strongly spatially variable (pressure and temperature dependent) material properties the standard dissipation number Di defined on the basis of the reference values may not be representative for a given model. We therefore also use an effective dissipation number Di_{eff} calculated as an average of the $\frac{\alpha(r) g_0}{c_p(r)}$ over the depth, where $\alpha(r)$ and $c_p(r)$ are horizontally averaged quantities. Similarly, we also define an effective Rayleigh number Ra_{eff}. The Nusselt number, a measure of a surface heat flux, is defined as:

$$Nu = \frac{\left\langle \frac{\partial T}{\partial z} \right\rangle}{\frac{\Delta T}{d}}. \tag{14}$$

It has been observed that the truncated version of the anelastic liquid compressible (TALA) models yield a heat balance mismatch - a small discrepancy between heat inflow and outflow (e.g. Jarvis and McKenzie, 1980; Leng and Zhong, 2008). This discrepancy is attributed to neglecting the dynamic pressure effect in the buoyancy term of the momentum equation (Leng and Zhong, 2008). This mismatch, up to a few percent, has however only negligible effect on the mantle dynamics and heat transport and is admissible for the present investigations, see also (Nakagawa and Tackley, 2010).

Our model configuration is based on a 2D Blankenbach-type model (Blankenbach et al., 1989) - with aspect ratio one rectangular domain and purely bottom heating. Impermeable free-slip is prescribed on all boundaries, at the bottom and top boundaries we prescribe constant temperature while both vertical boundaries have zero normal heat flux. Material parameters (density, expansivity, specific heat) are calculated using a multi-einstein lattice vibrational method (Jacobs et al., 2013, 2016) and interpolated from look-up tables (Jacobs and van den Berg, 2011). In order to benchmark our computational method based on P,T tabulated properties, we also carried out a set of simple convection experiments with parameterized properties where we also separate the effects of incompressibility from the combined effects of dissipation and adiabatic heating (see Appendix).

For the mantle material we chose a simplified mineralogy corresponding to an (magnesium endmember) olivine chemical composition Mg_2SiO_4 (Jacobs et al., 2016). For simplicity the low-pressure polymorphes of α, β, γ-olivine were not included. Instead an equivalent mechanical mixture of (post) perovskite (ppv/pv) $MgSiO_3$ and periclase (pc) MgO were used with mol fraction $X_{pv} = 0.5$ (weight fraction $W_{pv} = 0.71353$) for the full range of the mantle. The exothermic pv/ppv phase transition around 120 GPa and 2000 K was however taken into account. Further phase transitions in both ppv (Umemoto and Wentzcovitch, 2011) and pc (Karki et al., 1997) were ignored. Corresponding P,T dependent material properties are shown in Fig. 1. Thermal conductivity is constant in all model calculations - see Table 1.

In order to evaluate the effect of compressibility, we run several reference model cases in the extended Boussinesq approximation (Christensen and Yuen, 1985; Ita and King, 1994). These models have constant properties, ρ, c_p, set equal to the scale values specified in Table 1, and variable, depth-dependent thermal expansivity. We test two parameterised depth-dependent thermal expansivity profiles shown in Fig. 2. The first one, labeled as α_{depth1}, has expansivity with a parameterization adopted from (Hansen and Yuen, 1994; Steinbach and Yuen, 1995) (see Table 1), with a contrast value across the layer $\Delta\alpha$ that is set to 0.3. This expansivity of model α_{depth1} shows a decrease from a surface value of

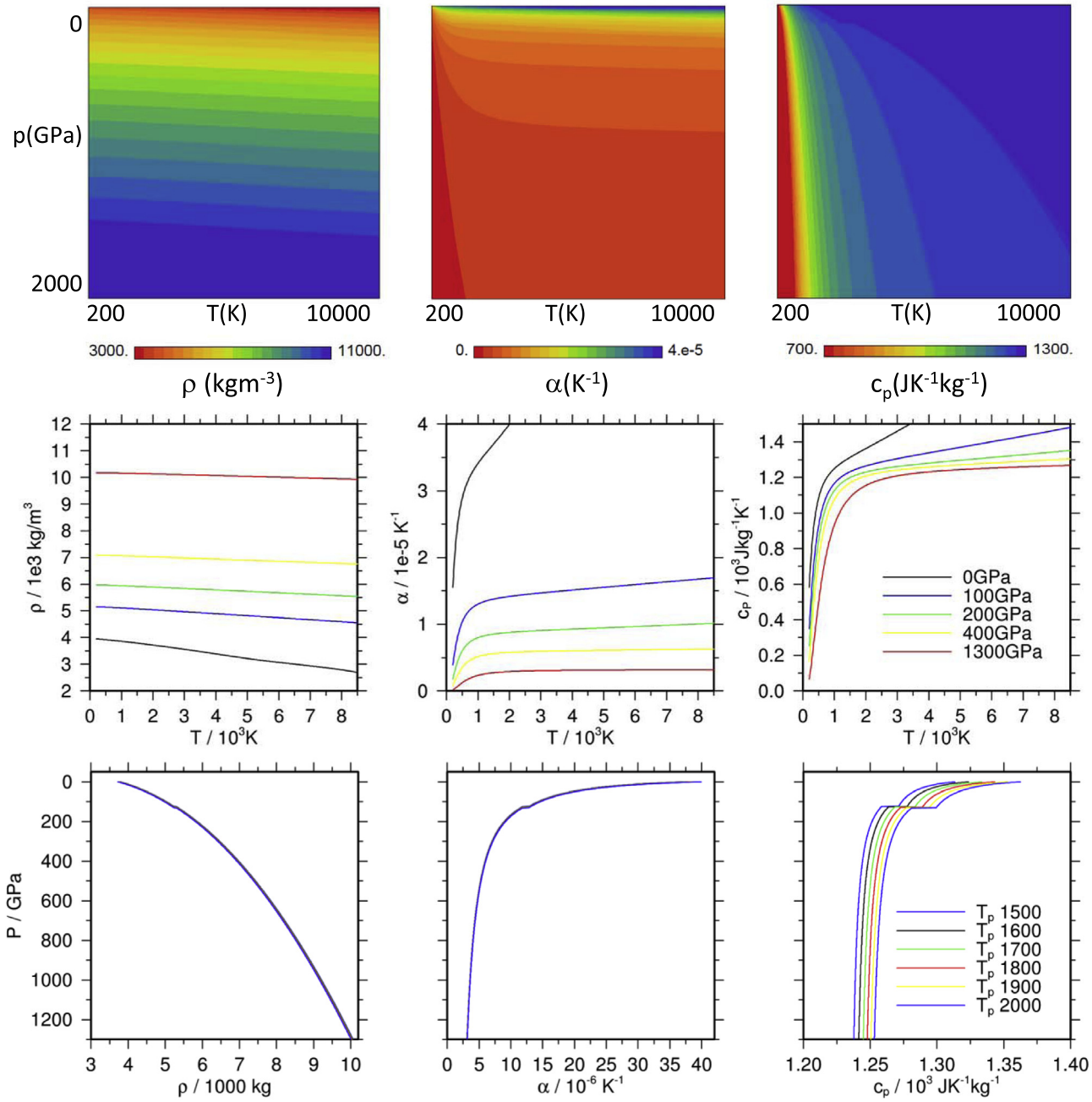

Fig. 1. Material parameters calculated using multi-einstein vibrational model as a function of pressure and temperature. Left column: density, middle column: thermal expansivity, right column: specific heat. The top row of frames shows the P,T distribution in the full range applied in the planetary mantle models. The second row illustrates the temperature dependence for several isobars with pressures specified in the legend. The bottom row shows corresponding adiabatic profiles for potential temperatures listed in the legend.

3×10^{-5} K^{-1} to 1×10^{-5} K^{-1} at the depth of 3100 km (mantle depth of the smallest planet) in agreement with mineral physics constraints (e.g. Chopelas and Boehler, 1992; Katsura et al., 2009). Below that depth (in case of larger planets with 2×, 4× and 8× Earth mass labeled as M2E – M8E) it remains constant (Fig. 2ab, yellow line). The second profile, labeled α_{depth2} (blue line in Fig. 2), is decreasing from the same surface value of 3×10^{-5} K^{-1} to 3×10^{-6} K^{-1} at the depth of 5800 km (mantle depth of the largest planet). For this second model the expansivity contrast $\Delta\alpha$ is 0.1. All EBA models have constant specific heat $c_p = 1250$ Jkg^{-1} K^{-1}. Symbols used are summarised in Table 1.

3. Model planets

Our modelling experiments were set up to represent thermal convection in terrestrial (rocky) exoplanets in the range of one to eight Earth masses, $M/M_E = 1, 2, 4, 8$, where compression of the mantle material is significant. Models of terrestrial planets subject to self compression were evaluated by solving coupled equations for the radial profiles of the spherically symmetric internal gravity and pressure (Sotin et al., 2010). An earthlike core mass fraction, $X_c = 0.3$, was applied in all models.

A simplified equation of state for the density of a purely iron core is adopted from (Tachinami et al., 2011). The choice of a

purely iron composition without lighter impurities such as sulphur results in a dense core model. For the silicate mantle we apply (P,T) tabulated material properties computed by a multi-einstein lattice dynamics method based on (Jacobs et al., 2013, 2016).

Resulting radial profiles of density, pressure, gravity and adiabatic temperature for the M1E-M8E planet models are shown in Fig. 3. The two sets of curves in Fig. 3d correspond to contrasting (surface) potential temperature of the adiabats $T_p = 1600$ K (curves with symbols) and $T_p = 2000$ K (solid lines). Frames (a-c) show overlay plots of profiles corresponding to both cases of mantle potential temperature. From the overlap of these curevs it is clear that the impact of potential temperature on the internal density, gravity and pressure distribution is insignificant. Characteristic parameter values for these four planets are listed in Table 2.

From these profiles follow the parameters of the four above mentioned planetary bodies: their mantle depth and surface gravity (Table 3). The gravity profiles vary by up to about 30% in the mantle. This appears to have however only a small effect on our

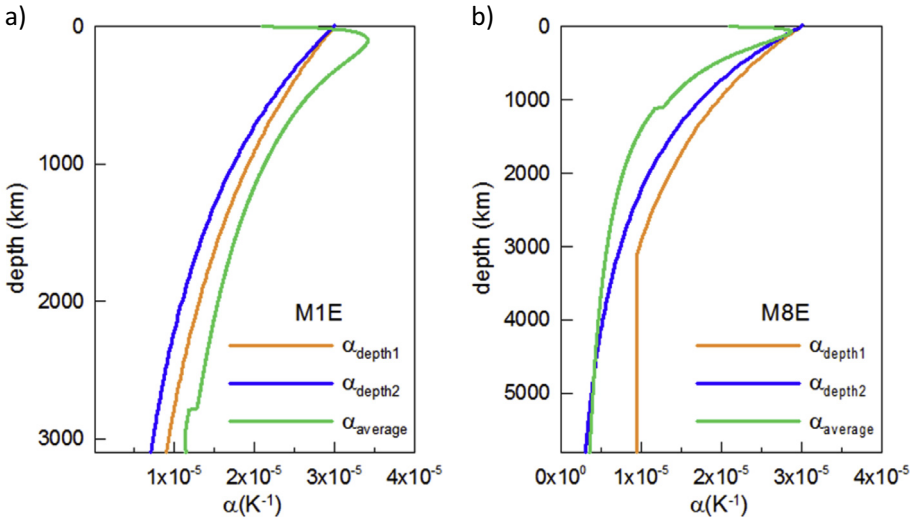

Fig. 2. Thermal expansivity used in EBA calculations. Parameterised profiles α_{depth1} (yellow line) and α_{depth2} (blue line) and a horizontally averaged expansivity of a TALA model with $Ra = 10^6$ (green line). Note that stepwise increase of expansivity due to pv-ppv phase transition occurs at different depths for the small and large planets due to higher pressure in the large body. (For interpretation of the references to colour in this figure legend, the reader is referred to the web version of this article.)

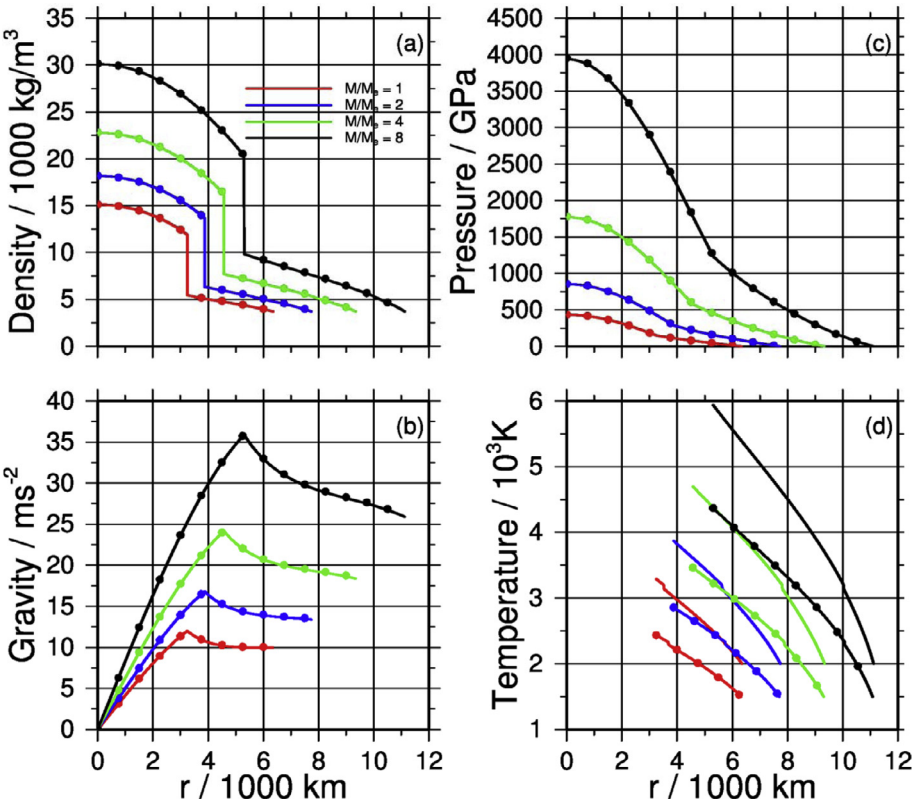

Fig. 3. Radial profiles of (a) density, gravity (b), pressure (c) and adiabatic temperature (d) for planet models with mass ranging from one to eight times the mass of the Earth. Results are shown for contrasting Mantle potential temperatures T_p of 2000 K (solid lines) and 1600 K (discrete symbols). Difference between both temperature cases are of the order of one percent.

Table 2
Characteristic parameter values of the planet models illustrated in Fig. 3. Mantle depth d, gravity acceleration at the surface and CMB, Mean (compressed) mantle density $\langle\rho_m\rangle$ and compression factor of the mantle, $C = \langle\rho_m\rangle/\rho(0, T_p)$. Where $\rho(0, T_p) = 3717$ kg/m^3.

M/M_E	d(m)	g_0 (m/s^2)	g_{CMB} (m/s^2)	$\langle\rho_m\rangle$ (kg/m^3)	C
1	3.102×10^6	9.95	12.0	4432	1.192
2	3.862×10^6	13.38	16.8	4842	1.303
4	4.768×10^6	18.37	24.2	5458	1.468
8	5.814×10^6	25.89	35.9	6407	1.723

Table 3
Model parameters: mass (in terms of Earth mass), mantle depth, surface gravity, temperature contrast across the mantle, viscosity, standard dissipation number, effective dissipation number, standard Rayleigh number, effective Rayleigh number and resulting Nusselt number.

Model	M/M_E	d(km)	g(ms^{-2})	ΔT(K)	$\eta_0(Pas)$	Di	Di_{eff}	Ra	Ra_{eff}	Nu
TALA-1E-10^4	1	3102	9.95	3800	9.43×10^{24}	0.52	0.46	10^4	1.20×10^4	3.89
TALA-1E-10^5	1	3102	9.95	3800	9.43×10^{23}	0.52	0.46	10^5	1.22×10^5	8.13
TALA-1E-10^6	1	3102	9.95	3800	9.43×10^{22}	0.52	0.46	10^6	1.23×10^6	14.06
TALA-1E-10^7	1	3102	9.95	3800	9.43×10^{21}	0.52	0.46	10^7	1.23×10^7	26.91
TALA-2E-10^4	2	3862	13.38	4600	2.97×10^{25}	0.86	0.61	10^4	1.08×10^4	3.46
TALA-2E-10^5	2	3862	13.38	4600	2.97×10^{24}	0.86	0.61	10^5	1.10×10^5	6.93
TALA-2E-10^6	2	3862	13.38	4600	2.97×10^{23}	0.86	0.61	10^6	1.11×10^6	12.50
TALA-2E-10^7	2	3862	13.38	4600	2.97×10^{22}	0.86	0.62	10^7	1.12×10^7	23.09
TALA-4E-10^4	4	4768	18.37	5400	8.99×10^{25}	1.47	0.78	10^4	0.99×10^4	3.06
TALA-4E-10^5	4	4768	18.37	5400	8.99×10^{24}	1.47	0.78	10^5	1.01×10^5	5.93
TALA-4E-10^6	4	4768	18.37	5400	8.99×10^{23}	1.47	0.79	10^6	1.02×10^6	9.68
TALA-4E-10^7	4	4768	18.37	5400	8.99×10^{22}	1.47	0.79	10^7	1.02×10^7	18.56
TALA-8E-10^4	8	5814	25.89	6600	2.81×10^{26}	2.52	0.99	10^4	0.93×10^4	2.73
TALA-8E-10^5	8	5814	25.89	6600	2.81×10^{25}	2.52	1.00	10^5	0.95×10^5	5.06
TALA-8E-10^6	8	5814	25.89	6600	2.81×10^{24}	2.52	1.00	10^6	0.96×10^6	8.05
TALA-8E-10^7	8	5814	25.89	6600	2.81×10^{23}	2.52	1.00	10^7	0.96×10^7	15.04
EBAaver-1E-10^4	1	3102	9.95	3800	9.43×10^{24}	0.52	0.47	10^4	0.91×10^4	3.46
EBAaver-1E-10^5	1	3102	9.95	3800	9.43×10^{23}	0.52	0.48	10^5	0.92×10^5	7.24
EBAaver-1E-10^6	1	3102	9.95	3800	9.43×10^{22}	0.52	0.48	10^6	0.93×10^6	12.56
EBAaver-1E-10^7	1	3102	9.95	3800	9.43×10^{21}	0.52	0.48	10^7	0.94×10^7	24.72
EBAaver-2E-10^4	2	3862	13.38	4600	2.97×10^{25}	0.86	0.61	10^4	0.71×10^4	2.93
EBAaver-2E-10^5	2	3862	13.38	4600	2.97×10^{24}	0.86	0.63	10^5	0.73×10^5	6.04
EBAaver-2E-10^6	2	3862	13.38	4600	2.97×10^{23}	0.86	0.63	10^6	0.73×10^6	10.18
EBAaver-2E-10^7	2	3862	13.38	4600	2.97×10^{22}	0.86	0.64	10^7	0.74×10^7	20.23
EBAaver-4E-10^4	4	4768	18.37	5400	8.99×10^{25}	1.47	0.78	10^4	0.53×10^4	2.43
EBAaver-4E-10^5	4	4768	18.37	5400	8.99×10^{24}	1.47	0.80	10^5	0.55×10^5	4.98
EBAaver-4E-10^6	4	4768	18.37	5400	8.99×10^{23}	1.47	0.81	10^6	0.55×10^6	8.15
EBAaver-4E-10^7	4	4768	18.37	5400	8.99×10^{22}	1.47	0.82	10^7	0.56×10^7	16.66
EBAaver-8E-10^4	8	5814	25.89	6600	2.81×10^{26}	2.52	0.98	10^4	0.39×10^4	1.96
EBAaver-8E-10^5	8	5814	25.89	6600	2.81×10^{25}	2.52	1.00	10^5	0.40×10^5	4.06
EBAaver-8E-10^6	8	5814	25.89	6600	2.81×10^{24}	2.52	1.02	10^6	0.41×10^6	6.92
EBAaver-8E-10^7	8	5814	25.89	6600	2.81×10^{23}	2.52	1.03	10^7	0.41×10^7	13.05

calculations. Therefore a uniform gravity acceleration (surface value) is used in all our calculations.

Mantle models are heated purely from below. The choice of a bottom boundary condition with prescribed temperature at the CMB is relevant for modelling planetary thermal evolution in models with mantle-core coupling through a heat-reservoir (van den Berg et al., 2005). In our present model set up for statistically steady state modelling without core coupling the bottom temperature T_{CMB} is derived from the temperature at the foot of a corresponding planet mantle adiabat T_{ad} increased by a temperature jump across the bottom thermal boundary layer ΔT_{bl}. This temperature jump is a free parameter in our model that defines the bottom boundary condition $T_{CMB} = T_{ad} + \Delta T_{bl}$. $\Delta\mathbf{T}_{bl}$ enters in the control parameter of the Rayleigh number through the temperature contrast across the convecting layer $\Delta T = T_{CMB} - T_S$. In order to limit the number of free parameters in our modelling set up we have set the parameter ΔT_{bl} to a reasonable value of 1000 K in all our models.

4. Results of numerical modelling

We performed numerical experiments to investigate heat transport in mantle convection under different pressure and temperature conditions relevant for terrestrial planets of one to eight earth masses. The planet mass, M, is used as a control parameter and the corresponding depth of the mantle, $d(M)$, enters in the (standard) dissipation number Di(M) (13). Besides the standard dissipation number, volume compression of mantle material also increases with planet mass M as shown in the ratio C of compressed and uncompressed mantle densities in Table 2. The other control parameter in our numerical experiments is the Rayleigh

number *Ra*. We have investigated the differences in heat transport characteristics between incompressible (Boussinesq) and compressible (TALA) thermal convection models. To this end time dependent model calculations were executed until steady state (typically in case of lower Ra and/or larger planet) or statistically steady state was reached. For cases resulting in a statistically steady state, we present time-averaged Nusselt numbers in the following.

Presentation of the results is split in two parts described in separate sub sections. The first part 4.1, deals with the effect of different formulations for the thermophysical properties density, thermal expansivity and specific heat at constant pressure in models with constant viscosity. In Section 4.2 we present results illustrating additional effects from variable pressure and temperature dependent viscosity on the convective heat transport.

4.1. Effect of compressibility on convective heat transport with uniform viscosity

In the first set of experiments we focuss on the role of the thermophysical properties, ρ, α and c_p. The uniform viscosity η_0 is derived from the given value of the standard Rayleigh number *Ra*. Characteristic parameters of the different models (including their viscosity scale value η_0) and resulting Nusselt numbers are listed in Table 3.

Fig. 4 shows a representative snapshot of the resulting temperature fields together with the corresponding distribution of the material properties. The depth/pressure dependent distributions are shown in corresponding profiles of horizontally averaged quantities. Results are shown for two compressible cases characterised with Ra $= 10^6$: Fig. 4a is for one Earth-mass body (M1E), Di $= 0.52$,

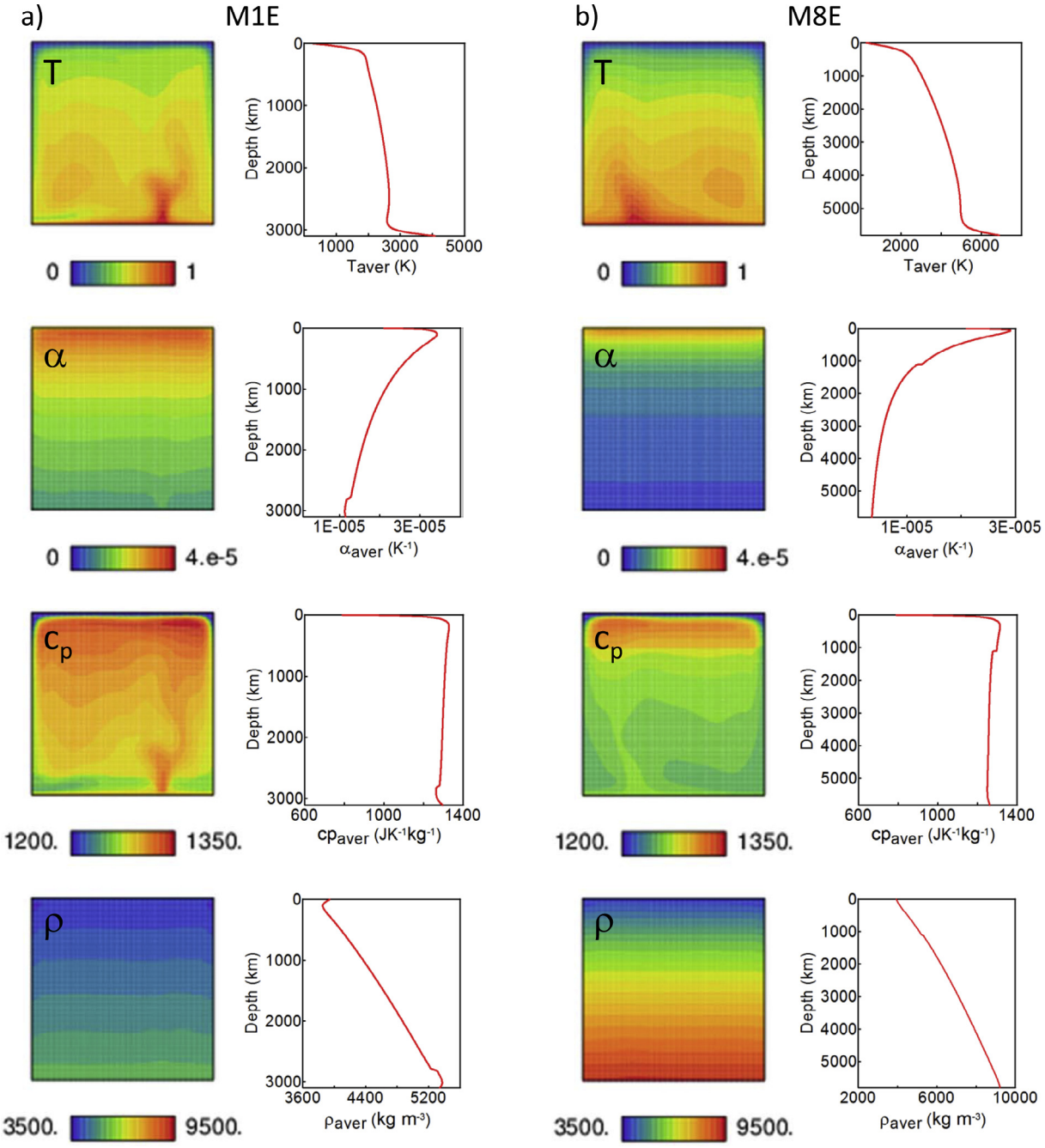

Fig. 4. One snapshot of model evolution in statistically steady state. (a) TALA model with *Ra* $= 10^6$ of an Earth-mass planet. Four rows show temperature, expansivity, specific heat and density in the whole model domain. (b) TALA model of M8E planet with *Ra* $= 10^6$.

while Fig. 4b shows results for a large planet (M8E), Di = 2.52. In both cases, the model calculation resulted in a statistically steady-state. The snapshots of the temperature field (top row) show a single hot upwelling and two cold downwellings on the sides for both model cases.

Thermal expansivity (second row from the top) is mostly controlled by pressure except of the upper thermal boundary layer where the temperature dependence is strongest, (Schmeling et al., 2003; Tosi et al., 2016). There it shows a local maximum, increasing from the cold surface with $\sim 2 \cdot 10^{-5}\,\mathrm{K}^{-1}$ to $\sim 3 \cdot 10^{-5}\,\mathrm{K}^{-1}$ at the bottom of the thermal boundary layer. Then the pressure effect prevails and expansivity is decreasing with depth and reaches the value of $\sim 1 \cdot 10^{-5}\,K^{-1}$, case (a)1ME and $\sim 0.5 \cdot 10^{-5}\,K^{-1}$ for case (b)8ME at the bottom of the model domain. Bottom pressure differs by a factor seven between cases (a) and (b). A small decrease of α can be identified in the verical profiles related to the pv-ppv transition at approximately 120 GPa, that occurs at different depths of ~2800 and ~1200 km in the smaller and larger planet respectively.

Specific heat (third row) is also mostly controlled by temperature just below the surface, where it reaches a low value of less than $800\,\mathrm{JK}^{-1}\,\mathrm{kg}^{-1}$. Then it increases rapidly with depth and remains nearly constant over most of the mantle ($\sim 1250\,\mathrm{JK}^{-1}\,\mathrm{kg}^{-1}$). At the pv-ppv transition specific heat drops by $\sim 20\,\mathrm{JK}^{-1}\mathrm{kg}^{-1}$.

Density (bottom row) increases from $3900\,\mathrm{kg\,m}^{-3}$ at the surface to $5350\,\mathrm{kg\,m}^{-3}$ (1ME) and $9227\,\mathrm{kg\,m}^{-3}$ (8ME), above the core-mantle boundary. A density increase at the pv-ppv transition is most clearly seen in the vertical density profile for the smaller planet model.

To evaluate the differencess between the compressible (TALA) models and incompressible models (both classical- and extended Boussinesq- approximation (BA or EBA)), horizontally averaged temperature profiles are shown in Fig. 5 for models with $\mathrm{Ra} = 10^6$ and contrasting planetary mass.

Fig. 5a presents results for a smaller planet model (M1E) for different model approximations (BA, EBA, TALA). The red profile corresponds to an incompressible classical Boussinesq (BA) model, with temperature increasing in both upper and lower thermal boundary layer and a nearly isothermal core of the mantle domain. The alternative incompressible extended Boussinesq (EBA) model with constant expansivity (purple line) produces a profile with approximately equipartitioning of the temperature contrast ΔT between the two thermal boundary layers and an adiabatic core of the domain.

When the incompressible model (EBA) is applied with depth dependent expansivity, both parameterised models α_{depth1} and α_{depth2} (blue and orange lines) yield very similar results. The decrease of the temperature gradient with increasing depth reflects the decrease of expansivity and corresponding adiabatic heating. The geotherms differ considerably from the incompressible (EBA) case with constant expansivity. The compressible model (black line) differs yet further from both parameterised EBA cases and has average temperatures that are higher than any of the other cases. The incompressible (EBA) with depth dependent expansivity is clearly a better approximation than EBA with constant properties or the classical Boussinesq (BA), but it is still more than 200 K off from the profile of the compressible model.

In the following we discuss whether these differences in the results are a consequence of different specifications of the compressible model, including P,T dependent properties, in particular α and c_p, compared to the incompressible models, including parameterised depth dependent properties, or whether the differences are due to the pressure dependence of density in the compressible model.

To that end we will apply an incompressible (EBA) model with depth-dependent expansivity $\alpha_{average}$ taken from a horizontally averaged expansivity of a corresponding compressible model. Expansivity in these models thus does not change with temperature and is fixed throughout the calculation. For the model with $\mathrm{Ra} = 10^6$ and for a small Earth-like planet M1E this expansivity profile is shown in Fig. 2a (green line). Specific heat is constant, fixed to a scale value of $1250\,\mathrm{Jkg}^{-1}\,\mathrm{K}^{-1}$. The resulting horizontally averaged geotherm in this model, labeled EBA$\alpha_{average}$, is shown in Fig. 5a (green line). The average expansivity profile $\alpha_{average}$ is close to both parameterised expansivity profiles α_1 and α_2 discussed above (cf. Fig. 2)a and similarly, the average geotherms are close to the average geotherms of the parameterised (EBA) runs - except of the uppermost mantle where the averaged expansivity has a more complex shape than both parameterised curves. The difference between the compressible model and its closest approximation (EBA$\alpha_{average}$) remains of the order of 200 K. In the case of the large (M8E) planet, the average expansivity profile $\alpha_{average}$ is

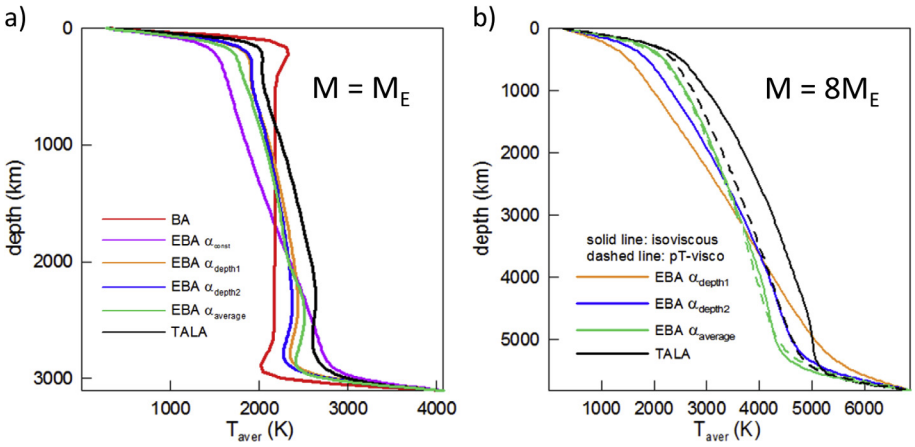

Fig. 5. (a) Horizontally averaged geotherms for Earth-mass (M1E) planet with $Ra = 10^6$ for following models: incompressible classical Boussinesq (red line), extended Boussinesq with constant expansivity (purple line), extended Boussinesq with depth dependent α_{depth1} (yellow line), α_{depth2} (blue line), extended Boussinesq with horizontally averaged expansivity from TALA model (green line) and compressible TALA model (black line). (b) The same for a large M8E planet, but only for extended Boussinesq models with depth-dependent expansivity and TALA model. Solid lines are for isoviscous models, dashed lines for models with pressure and temperature dependent viscosity. (For interpretation of the references to colour in this figure legend, the reader is referred to the web version of this article.)

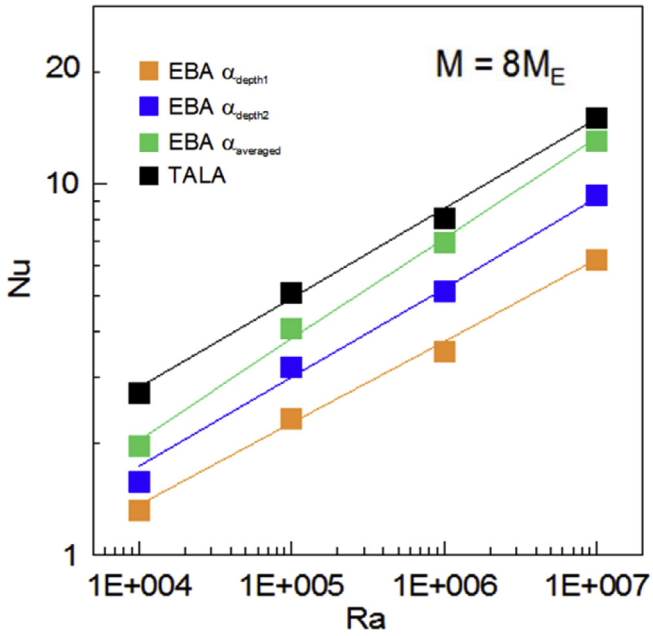

Fig. 6. Nusselt number as a function of standard Rayleigh number for the M8E planet. Yellow line is for EBA with α_{depth1} profile, blue line for EBA with α_{depth2} profile, green line for EBA$_{average}$ and black line for TALA model. (For interpretation of the references to colour in this figure legend, the reader is referred to the web version of this article.)

relatively close to the parameterised profile α_{depth2} in the uppermost mantle, they differ in the upper half of the mantle and are almost identical in the lowermost mantle (Fig. 2b). The parameterised profile α_{depth1} on the other hand gives a rather poor approximation of averaged expansivity, except perhaps for the uppermost mantle. Consequently, average geotherms (Fig. 5b) of the incompressible model with parameterised expansivity (EBAα_{depth2}) and the incompressible model (EBA$\alpha_{average}$) with averaged expansivity from the corresponding compressible run are rather close (green and blue lines).

The temperature of the incompressible model labeled α_{depth1} (orange line), on the other hand, is quite different from the above two. All incompressible model cases again show lower average temperature with respect to the compressible (TALA) model (black line) – by more than 500 K.

Heat transport efficiency is measured by the surface heat flux. Average geotherms of Fig. 5 suggest that the temperature gradient and corresponding heat flux resulting from different model approximations differ considerably. We demonstrate this in detail in Fig. 6, where Nusselt number (Nu) is plotted as a function of Rayleigh number for the above mentioned (in) compressible models of a large M8E planet. Nu increases with Ra according approximately a power-law relation. The highest Nu values are obtained for the compressible model (TALA). Incompresssible (EBA) models with parameterised expansivity show at most 60% of the (TALA) heat flux. The incompressible model with expansivity averaged from the compressible (TALA) run is closest to the compressible results, but even this model has a surface heat flux that is by $\sim 15\%$ lower than compressible model. Note that the above mentioned small misbalance between heat inflow and outflow attributed to TALA models is typically of the order of 3% and thus can by no means explain the difference that we observe between compressible and incompressible models.

Variation of the heat flux against the Rayleigh number is summarised in Fig. 7a for all planet models investigated - M1E (red), M2E (green), M4E (blue) and M8E (black). Squares show compressible models, diamonds are for incompressible models with hori-

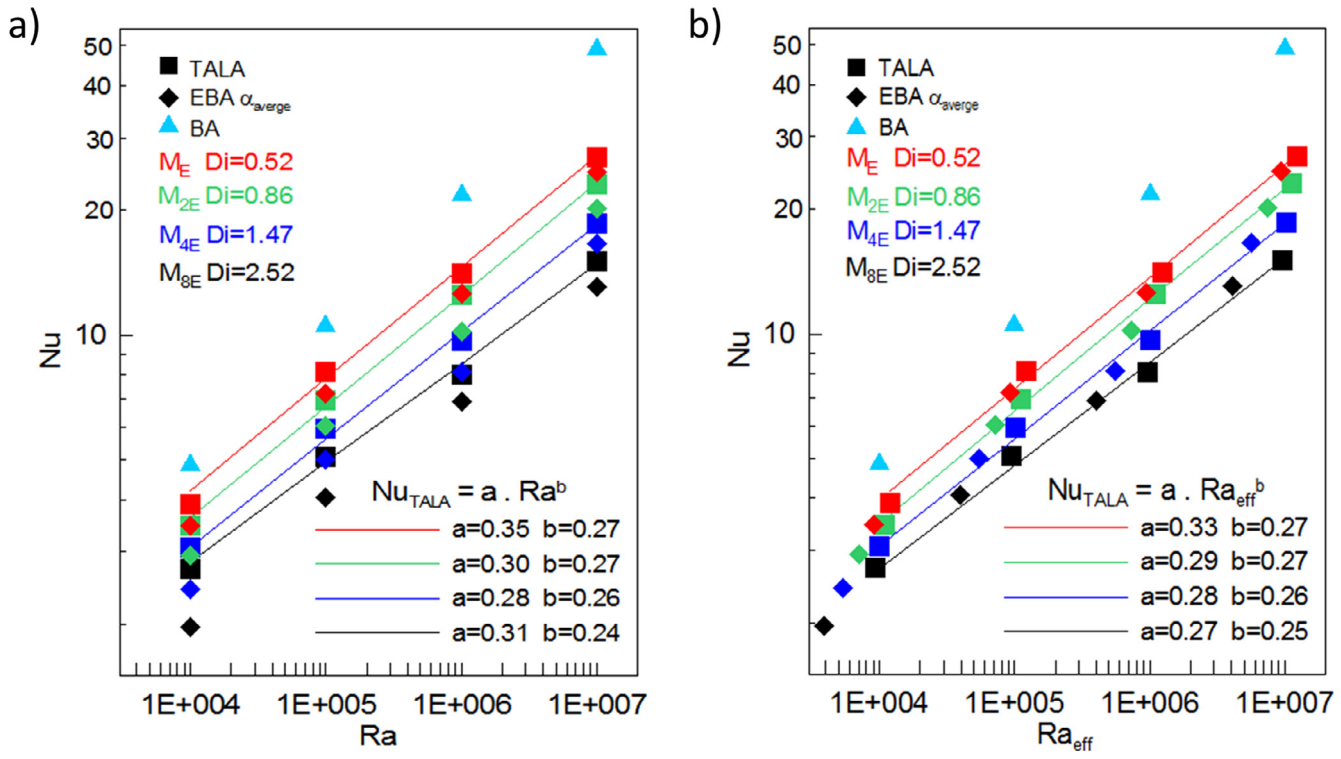

Fig. 7. (a) Nusselt number as a function of standard Rayleigh number for all planets considered: M1E (red), M2E (green), M4E (blue) and M8E (black). Squares are for TALA models, diamonds for corresponding extended Boussinesq models with horizontally averaged expansivity. Solid lines show power-law fit to TALA results. (b) The same as in panel (a), but now Nusselt number is a function of effective Rayleigh number. (For interpretation of the references to colour in this figure legend, the reader is referred to the web version of this article.)

zontally averaged expansivity taken from the corresponding compressible case. Clearly, the efficiency of convective heat transport, at a given Rayleigh number, decreases with increasing planetary mass. Larger planets (characterised by higher Di) show a lower heat flux. The same trend is observed for the incompressible cases, the latter ones however all show lower heat flux values than the compressible case. A powerlaw fit of the Nusselt number versus Ra relation for the compressible models gives $Nu \sim Ra^b$. Power index b changes slightly with planet size from 0.27 for the Earth-like planet to 0.24 for the largest planet considered. As the parameters that are used to evaluate Rayleigh number vary considerably within our model domains, especially for the large planets, we further show the variations of Nusselt number as a function of effective Rayleigh number Ra_{eff} (Fig. 7b). In compressible planets an increase of density with depth compensates the effect of decreasing expansivity when evaluating effective Rayleigh number and therefore the slope of the curves corresponding to TALA models has changed only slightly with respect to Fig. 7a (cf. parameter b shown in panels 7a and 7b). The effective Rayleigh number of extended Boussinesq models where density does not vary with pressure however differs from standard Ra significantly due to the decreasing expansivity. It is by 60% lower and consequently the EBA heat fluxes fall approximately on the same lines as those of TALA. This rescaling of the Nu(Ra) results underlines the key role of the density in explaining the different heat transport characteristics for compressible and incompressible models.

Next we examine in detail the heat transport efficiency dependence on planet size. To that end we present the Nusselt number as a function of the dissipation number for the models with $Ra = 10^6$ (Fig. 8). Note that we use here volume average dissipation number Di_{eff}. Standard dissipation number Di is significantly higher (cf. Table 3) as thermal expansivity decreases with depth. Results of compressible models are plotted with black squares labeled TALA, incompressible models with green diamonds labeled EBA. The lines show power-law fits to the model Nusselt numbers $Nu \sim c\ Di_{eff}^{-d}$. Compressible models show decay with exponent $d = 0.71$, Nusselt numbers of incompressible models decrease somewhat faster with $d = 0.80$. The contrast between the compressible and incompressible models increases with the dissipation or planet mass in line with the increasing degree of compression (Table 2).

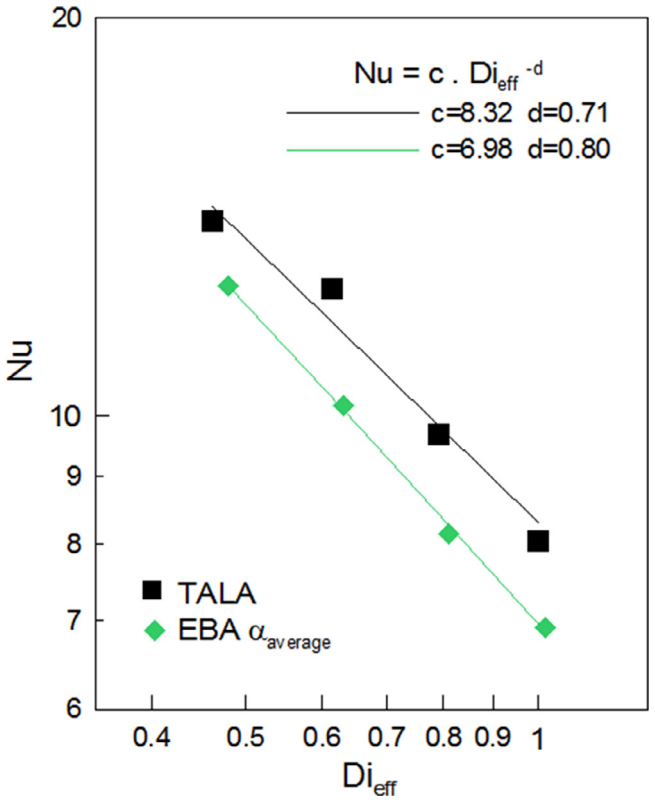

Fig. 8. Nusselt number as a function of Dissipation number for models with $Ra = 10^6$. Black squares are for TALA models, green diamonds are for corresponding EBA models with averaged expansivity and lines show the power-law fit. (For interpretation of the references to colour in this figure legend, the reader is referred to the web version of this article.)

4.2. Additional effect of variable viscosity on convective heat transport

In the previous section we considered models with uniform viscosity values. Since viscosity of solid state creep in silicate mantle materials is strongly temperature and pressure dependent (Karato, 2008), the results presented for isoviscous models may not be valid in case of variable rheology.

Therefore we have also done several convection experiments involving P,T dependent viscosity, to test if the higher heat transport capacity of compressible convection is also found in models with variable viscosity. For these experiments we adopt the viscosity model introduced in (Tackley et al., 2013) for the pressure and temperature regime of large terrestrial planets.

As before we consider planet models of different size of 1,2,4 and 8 Earth masses respectively. For the compressible (TALA) cases the thermophysical properties were kept the same as in the corresponding isoviscous model and the visocosity model was adapted according to (8).

For the incompressible (EBA) model cases we also modified the calculation of the static pressure in the evaluation of P,T dependent viscosity. Instead of calculating pressure from the uniform pressure gradient ρg for incompressible models it was here computed from the tabulated pressure depth profile of the corresponding compressible model case. Without this modification the evaluation pressure would be significantly lower in the EBA cases compared to the corresponding TALA cases. This would result in underestimation of the P,T dependent viscosity and make a meaningful comparison between incompressible and compressible models impossible.

Resulting Nusselt numbers of the model runs with variable viscosity are summarized in Table 4 with the corresponding standard Rayleigh numbers. The standard Rayleigh numbers shown here are based on the scale values of the parameters. The viscosity scale value η_0 was set to the reference viscosity $\eta_r = 1.9 \cdot 10^{21}$ defined in Table 1. The results show a similar contrast between the compressible and incompressible cases as observed in uniform viscosity models – the Nusselt numbers for the compressible cases are by 12–31 % higher. The average geotherms of the corresponding TALA and EBA models of the largest planet (M8E) with P,T dependent viscosity are further given in Fig. 5b. Similar to the uniform viscosity cases, the compressible model results here also in a warmer mantle than the incompressible one, but the magnitude of the difference is smaller. Straightforward comparison of the models is

Table 4
Models with pressure and temperature dependent viscosity. Standard Rayleigh number, Nusselt number of TALA model and Nusselt number of corresponding EBA model are given.

Model	Ra	Nu_{TALA}	Nu_{EBA}
M1E-pTvis	4.96×10^7	12.47	10.92
M2E-pTvis	1.56×10^8	12.68	10.44
M4E-pTvis	4.73×10^8	7.86	5.41
M8E-pTvis	1.47×10^9	6.83	5.68

however difficult in case of P,T dependent viscosity. Differences in temperature result in different volume average viscosities and Ra and therefore comparison of the corresponding TALA and EBA models is less straightforward as for uniform viscosity cases.

5. Discussion and Conclusions

We have investigated the effects of incompressibility on the heat transport capacity of Rayleigh–Benard convection in planetary mantles with emphasis on large terrestrial exoplanets of up to eight times the Earth's mass. In contrast to previous studies that apply models based on simplified parameterisations of material properties our approach is based on a selfconsistent, P,T dependent description of the thermophysical properties, density, thermal expansivity and specific heat, derived from a lattice vibrational mineral physics model. For the mineral composition of the model mantle we have taken a mixture of equal mol fractions of magnesium-endmember (post) perovskite and magnesio-wuestite, corresponding to an olivine (forsterite) chemical composition. Thus keeping the mantle material fixed we have varied the magnitude of gravitational compression by varying the mass of the planet keeping a constant Earthlike core mass fraction. This way the control parameter of the planetary mass is directly linked to the effective dissipation number through the depth of the convecting mantle. The Rayleigh number is the second control parameter that is set by the choice of the viscosity scale in our experiments.

Since thermal expansivity and heat capacity vary substantially both with pressure and temperature, it may be misleading to use the standard dissipation number based on the scaling parameters to characterise the effect of mantle compression. Therefore we use an effective dissipation number based on volume averaged properties in the presentation of the results and we show that for thermal expansivity and heat capacity of our mantle composition the dissipation number $Di_{eff} \sim 1$ for a large planet with $M = 8\ M_E$, significantly less than dissipation numbers in the range 3–5 usually assumed for large bodies based on surface parameters. Heat flux in our results then scales as $Nu \sim Di_{eff}^{-0.71}$. The powerlaw index of the Nusselt-Rayleigh number relation is similar for compressible and incompressible cases, $Nu \sim Ra^{0.27}$, with a small decrease for increasing planet mass.

Our experiments were focussed on the impact of the thermophysical properties in compressible models in comparison to incompressible Boussinesq models. Therefore we started from a simplified viscosity model ignoring pressure and temperature dependence where the viscosity value is used as a free parameter to tune the Rayleigh number. In case of a larger planet this implies that we define a higher viscosity for the same Rayleigh number. This means that the characteristic viscosity increases with the mass of the planet, for a given Rayleigh number. Such a viscosity dependence may be rationalised, if the viscosity was indeed increasing with pressure (Tackley et al., 2013) – we could thus expect higher volume average viscosity for larger bodies.

The results of our convection experiments show that the combined effect of adiabatic compression and viscous dissipation exerts significant effect on mantle heat transport. As a result the heat transport capacity expressed in the Nusselt-Rayleigh number relation decreases with increasing planetary mass or dissipation number in our compressible models in agreement with (Jarvis and McKenzie, 1980; Steinbach et al., 1989; Liu and Zhong, 2013).

In our results we find significant differences between incompressible (BA,EBA) and compressible (TALA) models in convective heat transport. The classical Boussinesq model (BA) overestimaties the heat transport capacity by a factor ~3 with respect to corresponding compressible TALA models. This is roughly in agreement also with the results of Liu and Zhong (2013), obtained for constant material properties, if we assume that effective Di of our large planet M8E is of the order of 1. This also agrees with results of Miyagoshi et al. (2014) who find a factor of 4 for a large compressible planet (ten Earth masses).

We also compare our compressible results with extended Boussinesq (EBA) models. Such comparison is important as the extended Boussinesq models are still extensively used in planetary convection modeling. We have shown that the incompressible EBA models with commonly used parameterised thermal expansivity systematically underestimate the heat transport capacity by about 40% compared to the corresponding compressible models. This descrepancy is reduced to ~ 15% by applying a horizontally averaged thermal expansivity, taken from a corresponding compressible model, in the incompressible EBA model. Furthermore the average mantle temperature is underestimated by more than 500 K by the incompressible (EBA) models.

To investigate additional effects from P,T dependent viscosity we also performed several model calculations including variable viscosity. The proper choice of a rheological model for the relevant P,T conditions of large terrestrial planets is not obvious and most available models use parameterizations based on extrapolations from rheological data obtained for lower P,T. Both temperature- (Miyagoshi et al., 2014; Miyagoshi et al., 2015) and pressure- (Stamenkovic et al., 2012; Tackley et al., 2013; Noack and Breuer, 2014) dependent viscosity have been tested in convection models of large exoplanets. The evidence for especially pressure effects on the viscosity is however ambiguous and there is not even an agreement as to whether viscosity should principally increase with pressure as for example in models with Arrhenius type P,T dependence with constant activation volume or whether it may decrease after reaching a viscosity maximum as a result of pressure weakening, (Karato, 2011; Stein et al., 2011; Tackley et al., 2013). In our additional experiments dealing with variable viscosity we have included the latter type model were viscosity reaches a maximum ('viscosity hill') in the deep mantle and decreases for further increasing pressure. This pressure weakening effect is parameterized in an activation volume that decreases with pressure in our parameterization adopted from (Tackley et al., 2013).

Our results show that surface heat flow values expressed in the Nusselt number are higher by at least 12 % in compressible convection models than in the corresponding incompressible models similarly to the isoviscous models discussed above. Direct comparison of the TALA and EBA models with P,T dependent viscosity is however problematic, as their pressure scales are very different. Here we adjusted the hydrostatic pressure in EBA models according to the corresponding TALA models – otherwise the pressure effects on viscosity would make the meaningful comparison impossible. Furthermore, the temperature differences between the two models result in different effective Ra, which again complicates straightforward comparison.

Other features that represent simplifications of our models are 2-D cartesian domain geometry and the constant thermal conductivity (van den Berg et al., 2005, 2010). These should be subject to further investigation. However we believe that our results show significant differences between the compressible and incompressible models that should be taken into account when modelling the thermal state of large terrestrial planets.

In conclusion we have found from our modelling: (1) in view of the large overestimation of convective heatflow, incompressible classical Boussinesq (BA) models should be avoided for modelling the thermal state of large planets were dissipation effects are significant. (2) incompressible (EBA) models that include the combined effects of adiabatic heating and viscous dissipation can be considered as a usefull first approximation for thermal modelling of planets. (3) Accounting also for the effect of incompressibility, included in TALA models, provides a further refinement to the

(EBA) models on the 10–20% level that will become more important on longer time scales, relevant for thermal evolution studies.

Acknowledgement

We thank Volker Steinbach and Ondřej Šrámek for fruitful discussions and two anonymous reviewers for constructive comments that helped to improve the manuscript substantially. Cooperation between H. Čížková and A. van den Berg has been supported through The Netherlands Research Center for Integrated Solid Earth Science (ISES). We further acknowledge support from the Grant Agency of Czech Republic under Grant No. 14-04145S.

Appendix A

In order to validate our computational methods we perform benchmark calculations for compressible media using uniform material properties. We investigate extensions of the steady state benchmark for incompressible convection by Blankenbach et al. (1989) for compressible media. Part of our results can then be compared with corresponding benchmark results of (King et al., 2010).

Models of compressible thermal convection commonly use parameterised material properties. In their benchmark studies Leng and Zhong (2008) and King et al. (2010) apply a similar formulation of the material model based on a common assumption that the Grueneisen parameter Γ is a constant $\Gamma = \frac{\alpha K}{\rho c_p} \equiv 1$. This is a special case of more general material models with uniform α, K, c_p and variable density where $\Gamma \sim \rho^{-1}$. With the Grueneisen parameter set to a constant value it is however no longer possible to vary the incompressibility or equivalently the 'compression scale height' $H_\rho = K/(\rho g)$ for a prescribed dissipation number Di. This follows from the defining expression for the Grueneisen parameter $\Gamma = H_\rho/H_T$, where $H_T = c_p/(\alpha g)$ is the thermal scale height. For given value of $Di = d/H_T$, prescribing Γ also fixes $K = \rho g H_\rho = \rho g \Gamma H_T$.

This makes it difficult to investigate the effects of compressibility separately from the dissipation effects on thermal convection in a general context where the incompressible EBA case with $1/K = 0, \Gamma \to \infty$ is an endmember. For this we need to be able to vary K independently from the dissipation number Di. This is relevant for a critical evaluation of the EBA approximation in mantle convection under high P,T conditions involving significant material compression. Therefore we take a different approach where we do not prescribe the Grueneisen parameter but instead vary incompressibility K indenpendent from the dissipation number Di.

In our benchmark we adopt the set up introduced by Blankenbach et al. (1989) for classical BA and later extended by Leng and Zhong (2008) and King et al. (2010) for EBA and for compressible TALA. Material properties were defined by uniform values for the incompressible Boussinesq models (BA,EBA). For the compressible (TALA) models only the pressure dependence of density is parameterized with a uniform isothermal incompressibility. For all model cases the density effect from thermal expansion is approximated by linearization.

With a uniform isothermal incompressibility K, pressure dependent density is parameterized as

$$\frac{1}{K} = \frac{1}{\rho}\frac{\partial \rho}{\partial P} = \frac{\partial \ln(\rho)}{\partial P}, \quad \rho(P) = \rho(P_0)\exp\left(\frac{P - P_0}{K}\right). \tag{15}$$

The thermal part is linearized at the reference isotherm $T_r = T_s$ (top surface temperature), and with $P_0 = 0, \rho(P_0, T_s) = \rho_0$ as follows:

$$\rho(P, T) = \rho_0 \exp\left(\frac{P}{K}\right)(1 - \alpha(T - T_s)) \tag{16}$$

Table 5
Nusselt number Nu and root-mean-square velocity Vrms for varying Di and K (infinity corresponds to incompressible cases BA and EBA).

Di	K(GPa)	Ra	Nu	Vrms
1.0	∞	10^4	2.2181	24.43
	∞	10^5	4.0326	108.9
	500	10^4	2.3778	25.81
	500	10^5	4.1383	106.7
0.50	∞	10^4	3.4020	33.99
	∞	10^5	6.9902	153.3
	200	10^4	3.8463	37.01
	200	10^5	7.7060	160.5
	167	10^4	3.9615	37.56
	167	10^5	7.8708	160.9
0.25	∞	10^4	4.1120	38.50
	∞	10^5	8.7709	174.1
	500	10^4	4.1692	39.72
	500	10^5	8.8923	179.4
	200	10^4	4.3493	40.63
	200	10^5	9.2303	182.1
	167	10^4	4.4133	40.95
	167	10^5	9.3501	183.0
0.0	∞	10^4	4.9110	43.08
	∞	10^5	10.706	194.1

We performed steady-state convection calculations in models with $Ra = 10^4$ and $Ra = 10^5$ ($\alpha = 3 \cdot 10^{-5}$ K^{-1}, $c_p = 1250$J kg^{-1}K^{-1}, $\rho_0 = 4 \cdot 10^3$kg m^{-3}). Incompressibility K ranges from 167 GPa to 500 GPa. The results are summarised in Table 5. For each value of Di several models with contrasting values of the incompressibility K are shown. The results for K = 167 GPa, ($\Gamma_0 = 1$), are close to the corresponding benchmark cases of King et al. (2010).

Concerning the different roles of incompressiblity and dissipation, we find from our results that the combined effects of adiabatic heating and viscous dissipation dominates over the effect of incompressibility, with Nusselt number decreasing with increasing dissipation number, $\partial Nu/\partial Di < 0$. This is in line with inferences of Steinbach et al. (1989). In contrast to this Nu shows a smaller increase when increasing compressibility $(1/K)$, from the incompressible EBA limit $(1/K = 0)$, such that $\partial Nu/\partial(1/K) > 0$.

References

Ammann, M.W., Brodholt, J.P., Dobson, D.P., 2010. Theoretical and computational methods in mineral physics: geophysical applications. Rev. Mineral. Geochem. 71, 201–224.

Batalha, N.M., Rowe, J.F., Bryson, S.T., Barclay, T., et al., 2013. Planetary candidates observed by Kepler. III. Analysis of the first 16 months of data. Earth and planetary. Astrophysics 204. http://dx.doi.org/10.1088/0067-0049/204/2/24.

Behounková, M., Tobie, G., Choblet, G., Cadek, O., 2010. Coupling mantle convection and tidal dissipation: applications to enceladus and earth-like planets. J. Geophys. Res. 115 (E14).

Blankenbach, B., Busse, F., Christensen, U., Cserepes, L., Gunkel, D., Hansen, U., Harder, H., Jarvis, G., Koch, M., Marquart, G., Moore, D., Olson, P., Schmeling, H., Schnaubelt, T., 1989. A benchmark comparison for mantle convection codes. Geophys. J. Int. 98, 23–38.

Chopelas, A., Boehler, R., 1992. Thermal expansivity in the lower mantle. Geophys. Res. Lett. 19, 1983–1986.

Christensen, U., Yuen, D.A., 1985. Layered convection induced by phase transitions. J. Geophys. Res. 90, 291–300.

de Vries, J., van den Berg, A., Westrenen, W., 2010. Formation and evolution of a lunar core from ilmenite-rich magma ocean cumulates. Earth Planet. Sci. Lett. 292, 139–147.

Foley, B.J., Bercovici, D., Landuyt, W., 2012. The conditions for plate tectonics on super-Earths: Inferences from convection models with damage, Earth Planet. Sci. Lett. 331, 281–290. http://dx.doi.org/10.1016/j.epsl.2012.03.028.

Fressin, F., Torres, G., Rowe, J.F., Charbonneau, D., et al., 2012. Two Earth-sized planets orbiting Kepler-20. Nature 482, 195–198.

Hansen, U., Yuen, D.A., 1994. Effects of depth-dependent thermal expansivity on the interaction of thermal–chemical plumes with a compositional boundary. Phys. Earth Planet. Inter. 86, 205–221.

Ita, J., King, S.D., 1994. Sensitivity of convection with an endothermic phase change to the form of the governing equations, initial conditions, boundary conditions and equation of state. J. Geophys. Res. 99, 15919–15938.

Jacobs, M.H.G., van den Berg, A.P., 2011. Complex phase distribution and seismic velocity structure of the transition zone: Convection model predictions for a magnesium-endmember olivine-pyroxene mantle. Phys. Earth Planet. Int. 186 (1–2), 36–48. http://dx.doi.org/10.1016/j.pepi.2011.02.008.

Jacobs, M.H.G., Schmid-Fetzer, R., van den Berg, A.P., 2013. An alternative use of Kieffer's lattice dynamics model using vibrational density of states for constructing thermodynamic databases. Phys. Chem. Miner. 40, 207–227.

Jacobs, M.H.G., Schmid-Fetzer, R., van den Berg, A.P., 2016. Phase diagrams, thermodynamic properties and sound velocities derived from a multiple Einstein method using vibrational densities of states: an application to MgO-SiO2. Phys. Chem. Miner. http://dx.doi.org/10.1007/s00269-016-0835-4.

Jarvis, G.T., McKenzie, D.P., 1980. Convection in a compressible fluid with infinite Prandtl number. J. Fluid Mech. 96, 515–583.

Karato, S.-I., 2008. Deformation of Earth Materials. Cambridge University Press.

Karato, S.-I., 2011. Rheological structure of the mantle of a super-Earth: some insights from mineral physics. Icarus 212 (1), 14–23. http://dx.doi.org/10.1016/j.icarus.2010.12.005.

Karki, B.B., Stixrude, L., Clark, S.J., Warren, M.C., Ackland, G.J., Crain, J., 1997. Structure and elasticity of MgO at high pressure. Am. Miner. 82, 51–60.

Katsura, T., Yokoshi, S., Kawabe, K., Shatskiy, A., Manthilake, M.A.G.M., Zhai, S., Fukui, H., Hegoda, H.A.C.I., Yoshino, T., Yamazaki, D., Matsuzaki, T., Yoneda, A., Ito, E., Sugita, M., Tomioka, N., Hagiya, K., Nozawa, A., Funakosh, K., 2009. P-V-T relations of MgSiO3 perovskite determined by in situ X-ray diffraction using a large-volume high-pressure apparatus. Geophys. Res. Lett. 36, L01305.

King, S.D., Lee, Ch., van Keken, P.E., Leng, W., Zhong, S., Tan, E., Tosi, N., Kameyama, M.C., 2010. A community benchmark for 2-D Cartesian compressible convection in the Earth's mantle. Geophys. J. Int. 180, 73–87. http://dx.doi.org/10.1111/j.1365-246X.2009.04413.x.

Leng, W., Zhong, S., 2008. Viscous heating, adiabatic heating and energetic consistency in compressible mantle convection. Geophys. J. Int. 173, 693–702. http://dx.doi.org/10.1111/j.1365-246X.2008.03745.x.

Liu, X., Zhong, S., 2013. Analyses of marginal stability, heat transfer and boundary layer properties for thermal convection in a compressible fluid with infinite Prandtl number. Geophys. J. Int. 194, 125–144. http://dx.doi.org/10.1093/gji/ggt117.

Mayor, M., Udry, S., Lovis, C., Pepe, F., Queloz, D., Benz, W., Bertaux, J., Bouchy, F., Mordasini, C., Segransan, D., 2009. The HARPS search for southern extra-solar planets. XIII. A planetary system with 3 super-Earths (4.2, 6.9, and 9.2 M). Astron. Astrophys. 493, 639–644.

Miyagoshi, T., Tachinami, Ch., Kameyama, M., Ogawa, M., 2014. On the vigor of mantle convection in super-Earths. J. Lett. 780 (L8).

Miyagoshi, T., Kameyama, M., Ogawa, M., 2015. Thermal convection and the convective regime diagram in super-Earth. J. Geophys. Res. Planets 120, 1267–1278.

Nakagawa, T., Tackley, P.J., 2010. Influence of initial CMB temperature and other parameters on the thermal evolution of Earth's core resulting from thermochemical spherical mantle convection. Geochem. Geophys. Geosyst. 11 (6). http://dx.doi.org/10.1029/2010GC003031.

Noack, L., Breuer, D., 2014. Platetectonics on rocky exoplanets: influence of initial conditions and mantle rheology. Planet. Space Sci. 98, 41–49.

Schmeling, H., Marquart, G., Ruedas, T., 2003. Pressure- and temperature-dependent thermal expansivity and the effect on mantle convection and surface observables. Geophys. J. Int. 154, 224–229.

Sotin, C., Jackson, J.M., Seager, S., 2010. Terrestrial Planet Interiors. In: Seager, S. (Ed.), Exoplanets, The University of Arizona Space Science Series.

Stamenkovic, V., Breuer, D., Spohn, T., 2011. Thermal and transport properties of mantle rock at high pressure: applications to super-Earths. Icarus 216, 572–596. http://dx.doi.org/10.1016/j.icarus.2011.09.030.

Stamenkovic, V., Noack, L., Breuer, D., Spohn, T., 2012. The influence of pressure-dependent viscosity on the thermal evolution of super-Earth. Astrophys J 748 (41). http://dx.doi.org/10.1088/0004-637X/748/1/41.

Stein, C., Finnenkotter, A., Lowman, J.P., Hansen, U., 2011. The pressure-weakening effect in super-Earths: consequences of a decrease in lower mantle viscosity on surface dynamics. Geophys. Res. Lett. 38 (L21201). http://dx.doi.org/10.1029/2011GL049341.

Steinbach, V., Hansen, U., Ebel, A., 1989. Compressible convection in the Earth mantle – a comparison of different approaches. Geophys. Res. Lett. 16, 633–636. http://dx.doi.org/10.1029/GL016i007p00633.

Steinbach, V., 1991. Numerische Experimente zur Konvektion in kompressiblen Medien. Universität zu Köln. PhD Thesis.

Steinbach, V., Yuen, D.A., 1995. The effects of temperature dependent viscosity on mantle convection with two mantle major phase transitions. Phys. Earth Planet. Int. 90, 13–36.

Tackley, P.J., Ammann, M., Brodholt, J.P., Dobson, D.P., Valencia, D., 2013. Mantle dynamics in super-Earths: post-perovskite rheology and self-regulation of viscosity. Icarus 225, 50–61.

Tachinami, C., Senshu, H., Ida, S., 2011. Thermal evolution and lifetime of intrinsic magnetic fields of super-Earths in habitable zones. Astrophys J 726 (70). http://dx.doi.org/10.1088/0004-637X/726/2/70.

Tachinami, C., Ogawa, M., Kameyama, M., 2014. Thermal convection of compressible fluid in the mantle of super-Earths. Icarus 231, 377–384.

Tosi, N., Maierova, P., Yuen, D.A., 2016. Influence of Variable Thermal Expansivity and Conductivity on Deep Subduction. Subduction Dynamics: From Mantle Flow to Mega Disasters, Geophysical Monograph 211, First Edition. Edited by Gabriele Morra, David A. Yuen, Scott D. King, Sang-Mook Lee, and Seth Stein, 115–133.

Umemoto, K., Wentzcovitch, R.M., 2011. Two-stage dissociation in $MgSiO_3$ post-perovskite. Earth Planet. Sci. Lett. 311, 225–229.

Valencia, D., O'Connell, R.J., Sasselov, D.D., 2006. Internal structure of massive terrestrial planets. Icarus 181. http://dx.doi.org/10.1016/j.icarus.2005.11.021, 545-554.

van den Berg, A.P., Rainey, E.S.G., Yuen, D.A., 2005. The combined influences of variable thermal conductivity, temperature- and pressure-dependent viscosity and core-mantle coupling on thermal evolution. Phys. Earth Planet. Inter. 149, 259–278.

van den Berg, A.P., Yuen, D.A., Beebe, G.L., Christiansen, M.D., 2010. The dynamical impact of electronic thermal conductivity on deep mantle convection of exosolar planets. Phys. Earth Planet. Int. 178, 136–154. http://dx.doi.org/10.1016/j.pepi.2009.11.001.

van Heck, H.J., Tackley, P.J., 2011. Plate tectonics on super-Earths: equally or more likely than on Earth. Earth Planet. Sci. Lett. 310 (3–4), 252–261. http://dx.doi.org/10.1016/j.epsl.2011.07.029.

van Summeren, J., Conrad, C.P., Gaidos, E., 2011. Mantle convection, plate tectonics, and volcanism on Hot Exo-Earths. Astrophys. J. Lett. 736, L15(6pp). http://dx.doi.org/10.1088/2041-8205/736/1/L15.